symmetry

IMPACT FACTOR 2.2

CITESCORE 5.3

Article

The Black Hole with a Finite-Sized Core Structure

Ting-Han Pei

Special Issue

Gravitational Physics, Black Holes and Space–Time Symmetry

Edited by

Dr. Yassine Sekhmani and Dr. Alexandre Landry

MDPI

https://doi.org/10.3390/sym17091431

symmetry

MDPI

Article

The Black Hole with a Finite-Sized Core Structure

Ting-Han Pei [1,2]

[1] Department of Electrical Engineering, Fu Jen Catholic University, New Taipei City 242062, Taiwan; 157328@mail.fju.edu.tw or thpei142857@gmail.com
[2] Institute of Astronomy and Astrophysics, Academia Sinica, Taipei 10617, Taiwan

Abstract

To meet the supergravity requirements of a black hole without a singularity, we propose some possible finite-sized core structures to avoid the confusing singularity problem. This research first studies the Coulomb repulsion between electrons at a distance of 10^{-15} m, where the inverse square of the distance is still workable, revealing that the energy of the entire observable universe is required to form a charged region with a radius of 50 m, including 1.4×10^{31} Coulomb electrons. Therefore, the existence of a singularity at the center of a black hole becomes physically unreasonable in this case. To avoid the singularity problem, we propose a finite-sized black hole core in which the inner core is composed of the vast majority of neutrons and a very small amount of ^{56}Fe. Under the conditions of a total charge of 1.648824×10^{20} C and a total mass equivalent to the Sun, a finite-sized black hole is constructed through this finite-sized core model. We use this non-rotating but charged, compact, star-like structure, surrounded by counter-rotating and co-rotating electrons, to construct a Kerr–Newman black hole with a finite-sized core structure. Based on this model, we can obtain the same spacetime as that of a traditional Kerr–Newman black hole.

Keywords: black hole; Schwarzschild radius; Kerr–Newman metric; geodesic; finite-sized core structure

PACS: 95.30.-k; 98.80.JK

Academic Editors: Alexandre Landry and Yassine Sekhmani

Received: 12 May 2025
Revised: 1 July 2025
Accepted: 4 July 2025
Published: 2 September 2025

Citation: Pei, T.-H. The Black Hole with a Finite-Sized Core Structure. *Symmetry* **2025**, *17*, 1431. https://doi.org/10.3390/sym17091431

1. Introduction

Some candidate black holes have been known for many years [1–3]. Although we do not know what the structure inside the black hole is like, we can make sure that mass is gathered in a small space with an invisible boundary, which is so-called the event horizon of the black hole. For a long time, the center of a black hole has been thought of as a singularity, where all mass and all charges gather. Massive particles, or light, are thought to be unable to escape the black hole due to ultra-strong gravity. But is this true for a photon or a massless particle? As we know, recent observation shows that a black hole moves quickly in one direction and leaves a trajectory including many stars in formation in space [4], revealing that such a black hole has a heavy, finite inner structure that generates super-gravitational fields around it. The zero dimension of the singularity inside a black hole seems to be unable to explain such a phenomenon.

Recently, gravitational waves from the mergers of binary black holes have been revealed using LIGO and VIRGO on several occassions [5–8]. Because the mass of each black hole exists within each event horizon, a merger means that two event horizons have to intersect with each other. Finally, their mass merged and energy equivalent to several solar

masses was released into space. The mass of the new black hole is less than the summation of the two original black holes. This raises a question: where does the lost mass go? The merger causes a collision between the two black holes, resulting in mass loss. The lost mass is transferred to other forms, such as gravitational waves and electromagnetic waves. These mergers seem to reveal that gravitational waves originate from the collisions of the inner structures of two black holes. Due to the variation in the total mass, the spacetime structure outside the new black hole is also different from that of the two black holes before the merger. If the gravitational waves are really confined in the black hole, the black hole behaves like a closed system, and the spacetime structure outside it does not change without the gravitational wave delivering some information about the variation in mass inside the black hole. In addition, another observation from a binary neutron star showed both receiving signals of gravitational waves and electromagnetic waves at almost the same time [9]. Since gravitational waves and electromagnetic waves originate from the same black hole and both follow the null geodesic in the same spacetime structure, we are curious about whether both gravitational waves and light can leave a black hole.

On the one hand, the singularity has a nonphysical infinite density in mass, charge, and energy; on the other hand, the merger of two black holes also implies the inner structure of the black hole to be a very high-density nucleus. This gives rise to another question about whether such a singularity is reasonable in a black hole or not. We have roughly discussed this problem in the past without rigorous physics [10]. In this research study, we first discuss this topic with respect to the characteristics of light in the black hole. Then, we consider energy conservation applied to a black hole and its previous star to propose a finite-sized nucleus in the black hole and discuss the limitations of core size. We reduce the inner structure of a black hole to a level that can be explained by standard physics. Finally, a Kerr–Newman black hole with a finite-sized core is proposed.

2. The Physical Finite-Sized Nucleus Model in the Black Hole

2.1. Introduction of the Schwarzschild Black Hole

Before obtaining a deeper understanding about the structure of the black hole, we first consider a non-rotating and uncharged black hole with a Schwarzschild radius $R_S = 2GM/c^2$, where M is the mass of the black hole, c is the speed of light in free space, and G is the gravitational constant. Its spacetime structure is described by the Schwarzschild metric, and there is one event horizon for this kind of black hole. The Schwarzschild metric [11–16] in the spherical polar coordinate (r, θ, ϕ) and the coordinate time t is expressed as follows:

$$\begin{aligned} \mathrm{d}s^2 &= e^{\nu(r)}c^2\mathrm{d}t^2 - e^{\lambda(r)}\mathrm{d}t^2 - \mathrm{d}\theta^2 - r^2\sin^2\theta\mathrm{d}\phi^2 \\ &= c^2\left(1-\tfrac{R_S}{r}\right)\mathrm{d}t^2 - \left(1-\tfrac{R_S}{r}\right)^{-1}\mathrm{d}r^2 - \mathrm{d}\theta^2 - r^2\sin^2\theta\mathrm{d}\phi^2, \end{aligned} \tag{1}$$

where the coordinate time t in a gravitational field is the time read by the clock stationed at infinity, because the proper time and coordinate time become identical there [15]. Then, we derive the propagation equation of light in this metric. Light propagates along the null geodesic with $\mathrm{d}s^2 = 0$, and the velocity of light in the Schwarzschild metric has been obtained [11–14], which is

$$\frac{1}{\left(1-\frac{R_S}{r}\right)^2}\left(\frac{\mathrm{d}r}{\mathrm{d}t}\right)^2 + \frac{1}{1-\frac{R_S}{r}}\left(r\frac{\mathrm{d}\theta}{\mathrm{d}t}\right)^2 + \frac{1}{1-\frac{R_S}{r}}\left(r\sin\theta\frac{\mathrm{d}\phi}{\mathrm{d}t}\right)^2 = c^2. \tag{2}$$

Considering light propagating along the radial direction with the radial velocity v_r [11,12,14,15], that is,

$$v_r^2 = \left(\frac{\mathrm{d}r}{\mathrm{d}t}\right)^2 = \left(1 - \frac{R_S}{r}\right)^2 c^2. \tag{3}$$

This yields $v_r = 0$ at $r = R_S$, where light has to spend infinite time passing through or leaving away from the event horizon. Because all our observations are made on the Earth, we have to use the viewpoint of a far observer to predict what we should "see" on the Earth according to the Schwarzschild metric or the black hole theory. Then, considering a massive test particle, the time spent from r_0 to R_S observed by a far observer on the Earth is as follows [14]:

$$\int_{r_0}^{R_S} \mathrm{d}t = \frac{A}{c}\int_{r_0}^{R_s} \frac{1}{\left(1 - \frac{R_S}{r}\right)\sqrt{A^2 - \left(1 - \frac{R_S}{r}\right)}}\mathrm{d}r = \infty, \tag{4}$$

where A is a constant between 0 and c. The integral in Equation (4) gives the infinite spending time from a finite distance r_0 to R_S. Therefore, the Schwarzschild metric or the black hole theory predicts that from the viewpoint of a far observer on Earth, nothing can enter the black hole, even if someone could wait 30 billion years, which is predicted by the black hole theory. Clearly speaking, this results in nothing passing through the event horizon into the black hole in finite time from the viewpoint of observations on Earth, far away from the black hole. Furthermore, according to the infinite redshift of light rays at the event horizon, it would even be unlikely to see any variation in the black hole, because no light information can be detected from the event horizon. However, this might create a problem. Recently, the Event Horizon Telescope (EHT) has shown images of the accretion disk of the M87 black hole [17]. The expansion and seeds of black holes have also been reported [18–20]. Therefore, the issue of whether the current black hole theory can explain the expansion of a black hole or not is pertinent. Following these ideas, we tried to use another metric to solve the problems outlined in this paper.

2.2. A Charged Sphere with a Radius of Fifty Meters and the Observable Universal Energy

In the following section, we propose a new perspective for a black hole to start solving the above problems. We begin by discussing the physical viewpoint of the structure of a black hole based on electrons and nuclear physics. All the above-mentioned research [21–29] was deduced from a mathematical viewpoint without any physical assumptions of material structures. If we review the evolution of a star in the final stage, we know that a star can become a white dwarf star, a neutron star, or a black hole, depending on its initial mass. In 1931, Chandrasekhar used special relativity and quantum statistical thermodynamics to find a non-rotating star with a mass limit of 1.4 $M_\odot$ (Chandrasekhar limit) due to electron-gas degenerate pressure [30,31]. Such a star is called a white dwarf star, which can collapse into a neutron star if its mass is slightly bigger than the Chandrasekhar limit [32]. This kind of neutron star was predicted to collapse further when its mass exceeds this limit. However, in 1939 and later, Oppenheimer and others, only based on the Pauli exclusion principle and neutron-neutron repulsion, first predicted that neutron stars would have another mass limit of approximately 0.7 $M_\odot$ (the Tolman–Oppenheimer–Volkoff limit) [32–34]. However, at that time, nuclear physics only considered Coulomb's and nuclear forces between neutrons, protons, and electrons, without strong interaction and any internal structures such as quarks and gluons. Until now, the collapse of a star to a black hole still follows the thoughts of one century ago. Before collapsing into a smaller size, the physical laws remain useful, and therefore, we have to consider energy conservation to see whether the collapse can be continuous to a

singularity or eventually stop at a certain size. Due to new physics, such as strong interaction, developed after the 1940s, we propose another way to emphasize the finite-sized core structure inside a black hole. The real material structure allows us to consider this viewpoint. Recently, proton experiments [35] showed that the inside pressure of a proton is as high as 10^{35} Pascals, and it is almost 10 times greater than the core pressure of a traditional neutron star. Such strong pressure indicates a great ability for the proton to bear a gravitational squeeze. Therefore, gravitational collapse is so unlikely that the internal structure of the black hole should be reconsidered. A recent report revealed that the equivalent mass-energy of the observable universe is about 1.3×10^{70} J [36]. Theoretically speaking, Coulomb's interaction shows a lot of necessary work completed or charges form a charged sphere [10]. Let us consider a case where pure 1.4×10^{31} Coulomb (C) electrons form a sphere. This many electrons have a mass of 7.96×10^{19} kg, and the Schwarzschild radius is $R_S = 1.18 \times 10^{-7}$ m. If these electrons are gathered from infinity to form a sphere with a radius of 50 m, as shown in Figure 1a,b, then the mass density is 1.52×10^{14} kg/m^3, which is within the density range of a white dwarf star, in which the inside pressure is supported by the degenerate pressure of the Fermi electron gas. According to the description in the Feynman Lectures Volume II [37], the inverse-square law of the Coulomb force is still a good approximation when the average distance between two charges is as small as 10^{-15} m. In our case, the average distance between two electrons is 2.25×10^{-15} m, which is larger than the criterion of 10^{-15} m. Thus, the self-energy of our case can still be appropriately calculated by classical electrodynamics. Here, we consider the additional charged case where Coulomb's interaction is calculated. The Reissner–Nordström metric for the exterior geometry is defined by [38–41]

$$ds^2 = c^2\left(1 - \frac{2GM}{c^2 r} + \frac{KGQ^2}{c^4 r^2}\right)dt^2 - \left(1 - \frac{2GM}{c^2 r} + \frac{KGQ^2}{c^4 r^2}\right)^{-1} dr^2 - d\theta^2 - r^2 \sin^2\theta d\phi^2. \quad (5)$$

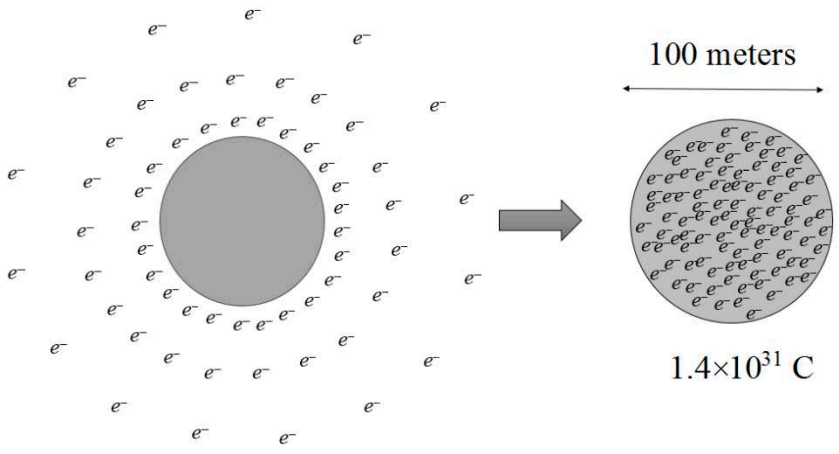

Figure 1. (**a**) A lot of electrons are moved together from infinity. (**b**) Pure 1.4×10^{31} Coulomb electrons gathering to form a sphere with a radius of 50 m. It needs energy more than 10^{70} J, which is the total energy in the observable universe.

By adopting the gravitational mass function M of a homogeneous star in the Reissner–Nordström metric, the equation yields the following [39,42,43]:

$$\frac{2GM}{c^2 r} = 1 - e^{\nu} + \frac{KGQ^2}{c^4 r^2}, \quad (6)$$

where Q is the total charge, and e^{ν} is a metric potential similar to that in Equation (1). Therefore, to move pure 1.4×10^{31} Coulomb electrons into a fifty-meter-radius sphere from infinity, one needs to complete the work against Coulomb's repulsive interaction to establish self-energy, which approximates the following [44]:

$$\begin{aligned} E_{self} &= \left(\frac{K}{G}\right)^{1/2} \int_0^R 4\pi c^2 \rho_e(r) \frac{\left[e^{\nu(r)} - 1 + \left(\frac{2GM}{c^2 r}\right)\right]^{1/2}}{2} dr \\ &\cong \int_0^R \frac{K\left[4\pi r^2 \rho_e(r) dr\right]}{r} \int_0^r 4\pi r'^2 \rho_e(r') dr' \\ &\cong \frac{3}{5} \frac{\left(8.987 \times 10^9\right)\left(1.4 \times 10^{31}\right)^2}{50} = 2.114 \times 10^{70}\ J, \end{aligned} \tag{7}$$

where the mass term can be ignored, and the charge density ρ_e is constant throughout the charged sphere. Thus, even if we use all the observable energy of the universe, theoretically speaking, we cannot shrink pure 1.4×10^{31} Coulomb electrons to a smaller space, even a single point. As we know, a black hole cannot obtain so much energy before collapsing or compressing everything into a singularity. Thus, in this case, the black hole has a finite-sized nucleus. The result is possibly used for the charged star.

2.3. A Charged White Dwarf Star Consisting of an Interacting Fermi Electron Gas

Since a lot of black holes evolve from stars with finite energy, the initial black hole should also have finite energy. Theoretically speaking, the black hole should have a finite-sized nucleus in it. Here, we adopt the part of the charged white dwarf model at absolute zero temperature where ϵN interacting Fermi electrons with $\epsilon \gg 1$ and $N/2$ helium nuclei coexist at the final stage of a superstar to prove it [45,46]. The volume of the star with a radius of R_0 is

$$V_0 = \frac{4}{3}\pi R_0^3, \tag{8}$$

and the total mass of the star is

$$M \approx (\epsilon m_e + 2m_n)N \approx 2m_n N, \tag{9}$$

where m_e is the electron mass, and m_n is the neutron mass. Then, at temperature $T = 0$ K, the total kinetic energy of the Fermi electron gas in the ultra-relativistic condition is as follows [46]:

$$U_e \approx \frac{2\pi V_0 m_e^4 c^5}{h^3}\left(\frac{p_f}{m_e c}\right)^4 = \frac{2\pi V_0 p_f^4 c}{h^3} = \frac{3\epsilon N h c}{4}\left(\frac{3\epsilon N}{8\pi V_0}\right)^{1/3} = \frac{3}{4}\epsilon N c p_f, \tag{10}$$

where the momentum of the Fermi electron is

$$p_f = h\left(\frac{3\epsilon N}{8\pi V_0}\right)^{1/3}. \tag{11}$$

The total kinetic energy of helium nuclei is almost zero, because they are Boson gas able to occupy the same lowest-energy state. The total energy of the star without Coulomb's energy at the final stage is

$$\begin{aligned} U_{total} &\approx U_e + \epsilon N m_e c^2 + 2N m_n c^2 + U_g \\ &\approx \frac{3\epsilon N h c}{4}\left(\frac{3\epsilon N}{8\pi V_0}\right)^{1/3} + \epsilon N m_e c^2 + 2N m_n c^2 + U_g, \end{aligned} \tag{12}$$

where the gravitational mass function M of a homogeneous star is as follows [39,42,43]:

$$\frac{2GM}{c^2 r} = 1 - e^{-\lambda} + \frac{KGQ^2}{c^4 r^2}, \tag{13}$$

where $e^{-\lambda}$ is one metric potential in the Reissner–Nordström metric. Therefore, for the uncharged case of $Q = 0$, the self-energy calculated by considering an inhomogeneous star with a radius of R is

$$U_g = \int_0^R 4\pi c^2 \rho(r) \frac{\left[1 - e^{-\lambda(r)}\right]}{2} dr = \int_0^R \frac{G\left[4\pi r^2 \rho(r) dr\right]}{r} \int_0^r 4\pi r'^2 \rho(r') dr'. \quad (14)$$

For the homogeneous white dwarf star, the above equation gives

$$U_g = \frac{3GM^2}{5R} \approx \frac{3G(2m_n N)^2}{5} \left(\frac{4\pi}{3V_0}\right)^{1/3}. \quad (15)$$

Later, we will use energy conservation to discuss whether the singularity model in the black hole is reasonable or not.

2.4. The Possible Black Hole Solutions of the Core Matter

Next, we consider one negatively charged case again, where some interacting Fermi electron gas exists at the center of the black hole, to check whether there could be a singularity at the center or not. This means negative charges are more prevalent than positive ones, and the center consists of a neutral part and the interacting Fermi electron gas. Equation (10) tells us that U_e has infinite energy when V_0 is close to zero. However, electron gas cannot become a singularity point because it needs infinite energy, as shown in Equation (6). When discussing gravitational collapse [11,12,14], the interacting Fermi electron gas serves as a good example to check whether gravitational collapse is reasonable or not [47].

Then, we use a neutron star to discuss another possibility—forming a black hole. General Relativity is important in the high-density regions of white dwarfs and neutron stars. Considering the spherically symmetric metric, the general relativistic equations of hydrostatic equilibrium include the Tolman–Oppenheimer–Volkoff (TOV) form [31,48–53]:

$$\frac{dp(r)}{dr} = -\frac{G}{r^2}\left[\rho(r) + \frac{p(r)}{c^2}\right]\left[m(r) + 4\pi r^3 \frac{p(r)}{c^2}\right]\left[1 - \frac{2Gm(r)}{rc^2}\right]^{-1}, \quad (16)$$

and

$$\frac{dm(r)}{dr} = 4\pi r^2 \rho(r). \quad (17)$$

When discussing a neutron star, neutrons play a main role. Theoretical studies of pure neutron matter derived from the nuclear many-body problem using two- and three-body potentials fitted to laboratory measurements of nuclear properties by experimental nucleon–nucleon (NN) scattering data indicate the density of nuclear matter inside a large nucleus as ^{208}Pb~n_s = 0.16 nucleon/fm^3 or $\rho_s = 2.7 \times 10^{14}$ g/cm^3 (=2.7×10^{17} kg/m^3) [33,51–53]. Based on these values, neutron stars are estimated to have densities up to ~$7\rho_s$ [33]. However, this reveals the prediction of the central pressure close to 625 MeV/fm^3 when the central density approximates $8.5\rho_s$, calculated by the hadronic equation of state (EOS) [33]. This central pressure value is equal to 10^{35} Pascals, which is the same as the inside pressure of the proton experimentally reported [35]. Therefore, we can expect the central density of a neutron star to be at least $8.5\rho_s$ when considering the pressure equilibrium. On the other hand, it is reported that one demonstration of the hadronic EOS consists of two poly -tropes (i.e., $p = p_0\rho^\gamma$) [33], where γ is the polytropic exponent, also called the adiabatic index [54]. The two exponents, $\gamma_1 = 4/3$, valid for the nuclear matter at densities below $\rho_s/3$, and $\gamma_2 = 3$, are connected at the transition pressure $p_t = p_n/8$ and baryon density

$\rho_s/2$, where the pressure p_n = 250 MeV/fm^3 = $10^{35.8}$ dyne/cm^2 [33]. These best-fit EOS parameters results in scaling between radius R and mass M as follows:

$$R \propto p_0^{1/(3\gamma-4)} M^{(\gamma-2)/(3\gamma-4)} \tag{18}$$

or

$$M \propto p_0^{1/(2-\gamma)} R^{(3\gamma-4)/(\gamma-2)}. \tag{19}$$

If the proportional constant K is considered in Equation (19), mathematically speaking, it will give possible conditions under which this neutron star becomes a black hole at $R = R_S$. Then, the R equation satisfying $R = R_S$ is given by

$$R_S = \frac{2GKp_0^{1/(\gamma-2)} R_S^{(3\gamma-4)/(\gamma-2)}}{c^2} \tag{20}$$

or

$$R_S = p_0^{-(2\gamma-2)} \left(\frac{c^2}{2GK}\right)^{(\gamma-2)/(2\gamma-2)}. \tag{21}$$

Explicitly, this expression reveals R_S is dependent on the proportionality of K and γ and has a singularity at $\gamma = 2$, which should be avoided and unused. When γ is determined, the smaller K is, the larger R_S. Besides this, there is another division using three-polytropic pieces to fit a fixed-region EOS [52–54]. In this piecewise–polytropic EOS, each piece is specified by two parameters, including the density ρ_i and the polytropic exponents γ_i for I = 1, 2, and 3 [52–54]. These six parameters, plus the core–crust transition density ρ_0, create a total of seven parameters used in this fitting EOS [52]. In these pieces, the pressure p and energy density ε are continuous everywhere, and the pressure and energy density within $\rho_i \geq \rho \geq \rho_{i\text{-}1}$, for i = 1–2, and $\rho \geq \rho_{i\text{-}1}$, for i = 3, satisfy the following [52–54]:

$$p(\rho) = p_i \left(\frac{\rho}{\rho_i}\right)^{\gamma_i} \tag{22}$$

and

$$\varepsilon = \frac{p}{\gamma_i - 1} + \left(\varepsilon_{i-1} - \frac{p_{i-1}}{\gamma_i - 1}\right) \frac{\rho}{\rho_{i-1}}, \tag{23}$$

where

$$\gamma_i = \frac{\ln(p_i/p_{i-1})}{\ln(\rho_i/\rho_{i-1})}. \tag{24}$$

A good fit is found for three polytropic pieces with fixed divisions at $\rho_1 = 1.85\rho_s$ and $\rho_2 = 2\rho_1 = 3.70\rho_s$ [54]. The third density boundary ρ_3 is chosen to be $2\rho_2$ [52,54]. Because $\rho_0 < \rho_1$ is required in this polytropic–piecewise EOS, the value $\rho_0 = 2 \times 10^{14}$ g/cm^3 is chosen as the first density parameter in the same study [53]. There is another choice of ρ_0 as $\rho_s/2.7$ or 10^{14} g/cm^3 [52]. The corresponding p_1, p_2, and p_3 for the EOS FPS are $10^{34.283}$, $10^{35.142}$, and $10^{35.925}$ dyne/cm^2, respectively [53]. The other parameters for the EOS AP3 are $10^{34.392}$, $10^{35.464}$, and $10^{36.452}$ dyne/cm^2, respectively [53]. Using these parameters, three polytropic exponents can be calculated for three polytropic pieces by applying Equation (24). Actually, not only *npeμ* matter has been discussed, but also hyperons, pions, Kaon condensate, and quark matter have also been shown the parametrized EOSs [53]. All the candidate EOSs perform very close to trends, and some of them even crisscross each other, as shown in Figure 2. Because the central pressure can be as high as 10^{35} Pascals or 625 MeV/fm^3, the corresponding central mass density is at least $8.5\rho_s$. The three-polytropic EOS is bound by $\rho_3 = 2\rho_2 = 7.4\rho_s$, which is below our requirement. The ρ-p relation is even considered the central density of $20\rho_s$ [51]. Therefore, for simplicity, we adopt a unified model to describe

the polytropic EOS for the neutron star as the red line plotted in Figure 2, and it can extend to $\rho > 9\rho_s = 2.43 \times 10^{15}$ g/cm^3. This polytropic EOS has the form

$$\log p - \log p_0 = \frac{4.2}{1.5}(\log \rho - \log \rho_0) \tag{25}$$

or

$$p = p_0 \left(\frac{\rho}{\rho_0}\right)^{2.8}, \tag{26}$$

where $\rho_0 = \rho_s/2.7 = 10^{14}$ g/cm^3 and $p_0 = 10^{32.7}$ dyne/cm^2 = 0.2485 MeV/fm^3. In addition, the $\gamma = 3$ polytropic EOS is denoted by the yellow line [51].

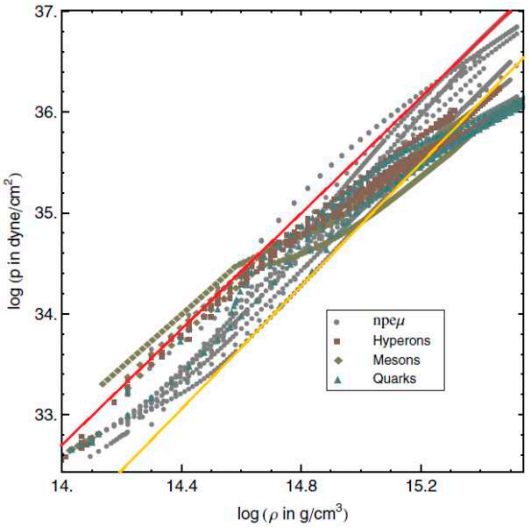

Figure 2. Pressure versus rest mass density for the set of candidate EOSs containing *npeμ* matter, hyperons, pion, Kaon condensates, and quark matter [54]. All these EOSs are performed close to each other, and some EOSs are even crisscrossed. For simplicity, we adopt a unified model to represent the p-ρ relation for the neutron star, which is drawn using a red line. The yellow line indicates the $\gamma = 3$ polytropic EOS (reuse and permissions license from the American Physics Society, 2025).

Then, Equation (26) gives

$$\frac{d\rho(r)}{dr} = -\left(\frac{dp}{d\rho}\right)^{-1} \frac{G}{r^2} \frac{\left[\rho(r) + \frac{p(r)}{c^2}\right]\left[m(r) + 4\pi r^3 \frac{p(r)}{c^2}\right]}{\left[1 - \frac{2Gm(r)}{rc^2}\right]}. \tag{27}$$

Equation (27) can be solved numerically as long as the central density is given. On the other hand, substituting Equation (26) into Equation (16) directly gives the m-ρ relation

$$m(r) = \left\{ \frac{\left[\frac{\rho(r) + \frac{p_0}{c^2}\left(\frac{\rho(r)}{\rho_0}\right)^{\gamma}}{\gamma \frac{p_0}{\rho_0}\left(\frac{\rho(r)}{\rho_0}\right)^{\gamma-1}\left(\frac{d\rho(r)}{dr}\right)}\right] 4\pi r \frac{p_0}{c^2}\left(\frac{\rho(r)}{\rho_0}\right)^{\gamma} + \frac{1}{G}}{\frac{2r}{c^2} - \left[\frac{\rho(r) + \frac{p_0}{c^2}\left(\frac{\rho(r)}{\rho_0}\right)^{\gamma}}{\gamma \frac{p_0}{\rho_0}\left(\frac{\rho(r)}{\rho_0}\right)^{\gamma-1}\left(\frac{d\rho(r)}{dr}\right)}\right]} \right\} r^2, \tag{28}$$

where $\gamma = 2.8$. Because $(d\rho/dr) < 0$ in the neutron star, the denominator is positive. Once $d\rho/dr$ in Equation (27) is obtained, then $m(r)$ in Equation (28) can be calculated, where $\rho(r)$ is evaluated by iteration based on the finite-difference method. In our simulations, the radial difference Δr of 10^{-3} m is used for calculations. This Δr is sufficiently convergent that the calculations of $\Delta r = 10^{-1}$ are almost the same as those of $\Delta r = 10^{-3}$. If the condition is satisfied, then the neutron star can be treated as a non-rotating and uncharged black

hole with a radius of r. Here, the Schwarzschild radius R_S is dependent on mass $m(r)$ and radius r. When equality in Equation (29) is considered, substituting Equation (28) into Equation (28) yields

$$r \leq \frac{2Gm(r)}{c^2} = R_S \tag{29}$$

which, when satisfied, the neutron star can be treated as a non-rotating and uncharged black hole with a radius of r. Here, the Schwarzschild radius R_S is dependent on mass $m(r)$ and radius r. When equality in Equation (29) is considered, substituting Equation (28) into Equation (27) gives

$$\left[\frac{\rho(R_S) + \frac{p_0}{c^2}\left(\frac{\rho(R_S)}{\rho_0}\right)^{\gamma}}{\gamma\frac{p_0}{\rho_0}\left(\frac{\rho(R_S)}{\rho_0}\right)^{\gamma-1}\left(\frac{d\rho(r)}{dr}\Big|_{r=R_S}\right)}\right]\left[1 + 8G\pi R_S^2\frac{p_0}{c^4}\left(\frac{\rho(R_S)}{\rho_0}\right)^{\gamma}\right] = 0, \tag{30}$$

If only the p-ρ relation like Equation (22) or Equation (26) is used, there is no solution of $\rho(R_S) = 0$ for the black hole for $\gamma \geq 2$, which is revealed in Equation (30). A reachable situation of $\rho(R_S) = 0$ at $r = R_S$ is given for $\gamma < 2$. One possibility for fixing this situation is to correct the expression of $P(r)$ by adding one or more terms of order n with $n < \gamma$. A simple correction is to add a term of $-kc^2\rho(r)$, where k is a positive constant, and then Equation (30) becomes

$$\left\{\frac{(1-k)\rho(R_S) + \frac{p_0}{c^2}\left(\frac{\rho(R_S)}{\rho_0}\right)^{\gamma}}{\left[\gamma\frac{p_0}{\rho_0}\left(\frac{\rho(R_S)}{\rho_0}\right)^{\gamma-1} - kc^2\right]\left(\frac{d\rho(r)}{dr}\Big|_{r=R_S}\right)}\right\}\left[1 - \frac{8G\pi R_S^2}{c^2}k\rho(R_S) + 8G\pi R_S^2\frac{p_0}{c^4}\left(\frac{\rho(R_S)}{\rho_0}\right)^{\gamma}\right] = 0, \tag{31}$$

and, mathematically speaking, it gives a few possible solutions, including one at $\rho(R_S) = 0$. Then, the m-ρ relation becomes

$$m(r) = \left\{\frac{\frac{\left[(1-k)\rho(r) + \frac{p_0}{c^2}\left(\frac{\rho(r)}{\rho_0}\right)^{\gamma}\right](4\pi r)}{\left(\gamma\frac{p_0}{\rho_0}\left(\frac{\rho(r)}{\rho_0}\right)^{\gamma-1} - kc^2\right)\left(\frac{d\rho(r)}{dr}\right)}\left[\frac{p_0}{c^2}\left(\frac{\rho(r)}{\rho_0}\right)^{\gamma} - k\rho(r)\right] + \frac{1}{G}}{\frac{2r}{c^2} - \left[\frac{(1-k)\rho(r) + \frac{p_0}{c^2}\left(\frac{\rho(r)}{\rho_0}\right)^{\gamma}}{\left(\gamma\frac{p_0}{\rho_0}\left(\frac{\rho(r)}{\rho_0}\right)^{\gamma-1} - kc^2\right)\left(\frac{d\rho(r)}{dr}\right)}\right]}\right\}r^2. \tag{32}$$

Except for $\rho(r) = 0$, the other possible zero solution in Equation (31) obeys

$$\left[1 - \frac{8G\pi R_S^2}{c^2}k\rho(R_S) + 8G\pi R_S^2\frac{p_0}{c^4}\left(\frac{\rho(R_S)}{\rho_0}\right)^{\gamma}\right] = 0, \tag{33}$$

or

$$(1-k)\rho(R_S) + \frac{p_0}{c^2}\left(\frac{\rho(R_S)}{\rho_0}\right)^{\gamma} = 0 \ (k > 1), \tag{34}$$

which can present the possibility of $m(R_S) = 0$ in Equation (32). Equation (34) gives a solution of a Schwarzschild black hole if we can find the mass density such that

$$\rho(R_S) = \left[(k-1)\frac{c^2}{p_0}\right]^{\frac{1}{\gamma-1}}\rho_0^{\frac{\gamma}{\gamma-1}}. \tag{35}$$

According to [55], a similar ad hoc term also appears in the MIT bag model, which would be a precedent and also a proof that our proposal is not groundless.

On the other hand, some demonstrations using Equation (33) are shown in Figure 3. One γ case is calculated and shown in Figure 3, where the central density ρ_c is between

$2.0 \times 10^{18.0}$ and $1.1 \times 10^{19.0}$ kg/m^3. When $m(r)$ in Equation (28) is applied, it is easy to accomplish by changing the value of γ. In this γ case, $\gamma = 2.80$ in Figure 3. The green line represents the star's radius where $r = R_S$. Since Equation (16) or (27) describes a non-rotating and uncharged star, $r = R_S$ is the limit of possible solutions due to the denominator. In Figure 3, $\rho_c = 8.0 \times 10^{19.0}$ kg/m^3 is exhibited, which corresponds to the furthest left curve, and $\rho_c = 1.1 \times 10^{19}$ kg/m^3 corresponds to the furthest right curve, so that the radius of the black hole at $\rho_c = 8.0 \times 10^{19.0}$ kg/m^3 is smaller than that at $\rho_c = 1.1 \times 10^{19.0}$ kg/m^3. In our calculations, the ratio of the star's radius to R_S is 1.14365 at $\rho_c = 1.1 \times 10^{19.0}$ kg/m^3 and 1.12547 at $\rho_c = 8.0 \times 10^{19.0}$ kg/m^3, and the ratio limitation is convergent to 9/8 = 1.125, as shown in the previous report [39].

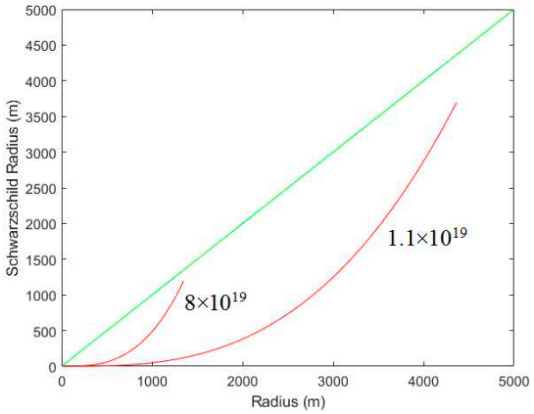

Figure 3. The calculations of the Schwarzschild radius R_S at different radii r according to the TOV equation, where ρ_c is $1.1 \times 10^{19.0}$ and $8.0 \times 10^{19.0}$ kg/m^3, respectively. The green line represents the black hole criterion, where the star's radius $r = R_S$. The two r-R_S relations consider the parameters of $p_0 = 10^{32.7}$ dyne/cm^2, $\rho_0 = \rho_s/2.7 = 10^{14.0}$ g/cm^3, and $\gamma = 2.8$.

2.5. Proposing a Possible Black Hole with a Finite-Sized Core Structure

When considering the charged effect, the exterior spacetime of a charged star can be described by the Reissner–Nordström metric [38–43,56–60]. The Einstein–Maxwell stress tensor of the isotropic fluid and electromagnetic field in terms of the Faraday–Maxwell tensor $F_{\mu\nu} = \partial_\mu A_\nu - \partial_\nu A_\mu$ is as follows [39,41,42,56,57,59,60]:

$$T_\nu^\mu = \left(P + \rho c^2\right) u^\mu u_\nu + P\delta_\nu^\mu + \frac{1}{4\pi}\left(F^{\mu\alpha}F_{\alpha\nu} - \frac{1}{4}\delta_\nu^\mu F^{\alpha\beta}F_{\alpha\beta}\right), \tag{36}$$

where A_μ is an electromagnetic four potential, u^μ is the contravariant four-velocity of the fluid, ρc^2 is the energy density of the fluid, and P is the isotropic pressure in the fluid. With the electric charge density ρ_e in the matter, the total charge is as follows [40–43,56,57]:

$$Q(r) = r^2 E(r) \int_0^r 4\pi r'^2 \rho_e(r') \left[1 - \frac{2Gm(r')}{c^2 r'} + \frac{KGQ^2(r')}{c^4 r'^2}\right]^{-1/2} dr'. \tag{37}$$

The above gravitational mass $m(r)$ inside the sphere of radius r represents the energy conservation measured in the star's frame. One can find that another of Einstein's equations gives a differential equation for $m(r)$ [38,39,56,59,60]:

$$\frac{dm(r)}{dr} = 4\pi\rho(r)r^2 + \frac{KQ(r)}{c^2 r}\frac{dQ(r)}{dr}. \tag{38}$$

Since $m(r)$ represents the gravitational mass inside the sphere of radius r, Equation (38) represents the energy conservation measured in the star's frame [39]. Using the covariant conservation of the mass–energy stress tensor, $T_\nu{}^\mu{}_{;\mu} = 0$, one gets the hydrostatic equilib-

rium equation that determines the global structure of electrically charged stars. Then, we obtain the modified TOV equation as follows [39,41–43,56,59,60]:

$$\frac{dP(r)}{dr} = -\frac{2G}{r^2}\left(\rho(r) + \frac{P(r)}{c^2}\right)\frac{\left[m(r) + \frac{4\pi r^3}{c^2}\left(P(r) - \frac{KQ^2(r)}{4\pi c^2 r^4}\right)\right]}{\left[1 - \frac{2Gm(r)}{c^2 r} + \frac{KGQ^2(r)}{c^4 r^2}\right]} + \frac{KQ(r)}{4\pi r^4}\frac{dQ(r)}{dr}. \tag{39}$$

Furthermore, if an incompressible fluid is considered, $\rho(r)$ is a constant throughout the body. Therefore, the energy density is also constant in the whole star. Based on this, the small electric-charge effect on mass is discussed next. As mentioned before, the zero-charge case in the Reissner–Nordström metric corresponds to the interior Schwarzschild structure. When a few electric charges exist in the star, the mass distribution is perturbed according to Equation (38). Then, the charge $Q(r)$ is treated as a small perturbation, and mass and charge take the following forms [39]:

$$Q(r) = Q_1(r) \tag{40}$$

and

$$m(r) = m_0(r) + m_1(r), \tag{41}$$

where $m_0(r)$ is the mass of the uncharged star, and $Q_1(r)$ and $m_1(r)$ are the perturbed small charge and mass distributions to be determined. Equation (41) reveals that the total mass in the electric-charge case is more than in the uncharged case. Thus, the increasing mass can improve the optimized ratio of r to R_S when a few electric charges are in the neutron star. Next, we can define a characteristic length, R_c, as follows [39]:

$$R_c^2 = \frac{3c^2}{8\pi G\rho}, \tag{42}$$

then, the r-dependent mass within the sphere of radius r is

$$m_0(r) = \frac{c^2 r^3}{2GR_c^2} = \frac{c^2 R_c}{2G}\left(\frac{r}{R_c}\right)^3 = \frac{c^2 R_c}{2G}x^3, \tag{43}$$

where a dimensionless variable $x = r/R_c$ is introduced. It has been proved that the so-called Schwarzschild limit in an uncharged and non-rotating star yields the following [39]:

$$\frac{c^2 R}{GM} = \frac{2R}{R_S} = \frac{9}{4}, \tag{44}$$

which is the same as the limit of our simulations that $R/R_S = 1.125$. Even more, a similar upper-ratio limit for the charged and non-rotating star has been given by the following [41,61]:

$$\frac{R_S}{2R} \leq \left[\frac{2R^2 + 3\left(\frac{KGq^2}{c^4}\right)}{9R^2} + \frac{2}{9R}\sqrt{R^2 + 3\left(\frac{KGQ(R)^2}{c^4}\right)}\right], \tag{45}$$

where $Q(R)$ is the total charge of the star. Suppose the electric charge density is proportional to the energy density in the small-charged effect, that is,

$$\rho_e = \alpha\sqrt{\frac{G}{K}}\rho, \tag{46}$$

where α is a proportional constant. Then, the electric-charge distribution is given by the following [39]:

$$Q_1(x) = \frac{3}{4}\alpha\left(\sin^{-1}x - x\sqrt{1-x^2}\right), \tag{47}$$

and the mass distribution is as follows [39]:

$$m_1(x) = \frac{3}{8}\alpha^2\left(3x - x^3 - 3\sqrt{1-x^2}\sin^{-1}x\right), \tag{48}$$

if natural units $K = G = c = 1$ are used. Finally, Equation (44) becomes

$$\frac{Rc^2}{GM} = \frac{9}{4} - 1.529\alpha^2. \tag{49}$$

In Equation (49), it seems that $\alpha = 0.4044$ gives the value on the right side equal to 2.00 but is out of the small-charge range. Actually, it has been pointed out that this quasiblack hole configuration is given by the extremal charged case where α is as high as 0.99 [38]. On the other hand, a smaller value has been reported for a similar case, a charged perfect fluid model with high compactness [55]. In this model, the minimum value in Equation (45) gives

$$\frac{1}{u_{max}} = \frac{c^2R_{min}}{GM} = \frac{2R_{min}}{R_S} = \frac{1}{0.5337972212} = 1.87337 < 2, \tag{50}$$

in which the radius of the compact star is smaller than the Schwarzschild radius. In this minimum condition, the total charge is $Q(R_{min}) = 1.648824 \times 10^{20}\ C$, and the larger event horizon is

$$r_+ = \frac{GM}{c^2} + \sqrt{\frac{G^2M^2}{c^4} - \frac{KGQ(R_{min})^2}{c^4}} \approx 1.194\frac{GM}{c^2} = 0.597R_S, \tag{51}$$

where $M = M_\odot$. In this reported case, $r_+ < R_{min} < R_S$. According to this, a double-characteristic structure, based on the perfect fluids, is proposed to explain the existence of the black hole, as shown in Figure 4. This kind of black hole has a total charge of zero or nonzero and may have three regions or more. In this structure, the inner region, denoted by I, is a positively charged region, and almost the whole mass of the black hole exists here. The middle region, denoted by II, is a region including negative charges, such as electrons. The outermost region, denoted by III, is another negatively charged layer, and both Region II and Region III can balance the positive charges in Region I. The advantage of the composition of Region II and Region III in forming a black hole is the electron, because its mass is only about 9.1×10^{-31} kg. However, there is a very strong Coulomb attraction between Region I and Region II and Region III. If electrons in Region II and Region III are initially at rest, they will be quickly attracted toward Region I. Therefore, electrons of Region II and Region III aim to move ultra-relativistically around Region I and move corotating or counter-rotating, respectively. This situation is similar to the M87 black hole surrounded by a hot disk accretion [17].

On the other hand, the possible constitutions in Region I are mostly neutrons with a few Fe nuclei, ^{56}Fe. The appropriate metric used in Region I, Region II, and Region III is the Kerr–Newman metric [62] for all possible cases in the three regions. On the other hand, the appropriate metric outside Region III is also the Kerr–Newman metric [63] because all charges enclosed by the outer dashed circle could be zero or nonzero, and the total angular momentum could also be zero or nonzero. Therefore, the charged term $R_{Q,new}$ and the rotation term a_{new} of the finite-size core structure are zero or nonzero, depending on the conditions of Region II and Region III. The whole negative charges in Region II

and Region III are supposed to move in circular orbitals, corotating and counter-rotating, respectively. Because the minimum radius is $R_{min} = 0.9367R_S$ for the case of the total charge $Q = 1.648824 \times 10^{20}$ C [55], these negatively charged regions have to exist between R_{min} and R_S to ensure that the whole structure is within the Schwarzschild radius R_S and satisfies the requirement of a Schwarzschild black hole, where $R_{Q,new}$ and a_{new} are both zero. The equatorial motions of charged test particles in the Kerr–Newman metric have been studied [63–67], in which the case of $l = 0$ in the Kerr–Newman–Taub–NUT metric is also used in our research here. Based on these reports [63–67], our model has strong support.

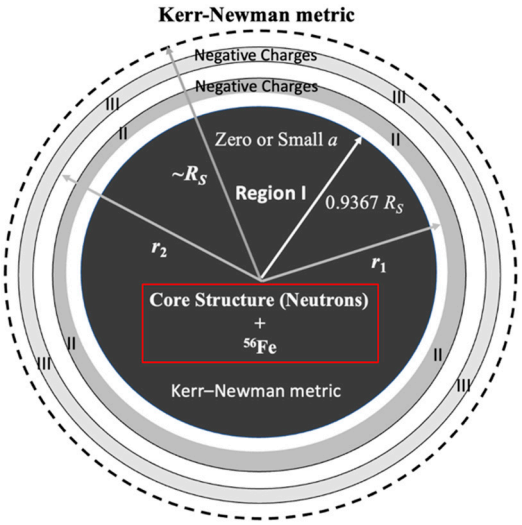

Figure 4. The cross-section structure of a double-characteristic black hole with a total charge of zero or nonzero. This kind of black hole has a positively charged Region I, possibly consisting of neutrons with a few Fe nuclei specially marked by red frame, which is surrounded by negative charges corotating or counter-rotating, such as electrons, denoted by Region II. Their outermost thin layer consists of negative charges, denoted by Region III. These negative charges, such as electrons, may move corotating or counter-rotating around Region I and Region II. If electrons move corotating in Region II, then they move counter-rotating in Region III, and vice versa. The total negative charges in Region II and Region III balance the total positive charges in Region I. The appropriate metric used in all space, including Region I, Region II, and Region III, is the Kerr–Newman metric for all possible cases in three regions. Both Region II and Region III exist between $0.9367R_S$ and R_S, in which the minimum radius $R_{\min} = 0.9367\ R_S$ of Region II and the total positive charge $Q = 1.648824 \times 10^{20}$ C in Region I are considered here [55]. Due to this structure of the black hole, the radius of Region III is required to be smaller than the outer event horizon $r_+ = \left(R_S + \sqrt{R_S^2 - 4a_{new}^2 - 4R_{Q,new}^2}\right)/2$, which is one of the criteria of a Kerr–Newman black hole. Therefore, a black hole of a finite-size core structure is reached by our model.

Then, we start with the Kerr–Newman metric to discuss the model mentioned above. This starting point is chosen because Region III includes rotating charges, so it is better to describe the spacetime using the Kerr–Newman metric than the Reissner–Nordström metric. The Kerr–Newman metric is as follows [25,44,68]:

$$\begin{aligned} ds^2 = \tfrac{\Delta - a^2\sin^2\theta}{\rho^2}c^2dt^2 - \tfrac{\rho^2}{\Delta}dr^2 - \rho^2 d\theta^2 + 2ac\sin^2\theta\left(1 - \tfrac{\Delta - a^2\sin^2\theta}{\rho^2}\right)dtd\phi \\ -\left[\rho^2 + a^2\sin^2\theta\left(2 - \tfrac{\Delta - a^2\sin^2\theta}{\rho^2}\right)\right]\sin^2\theta d\phi^2, \end{aligned} \tag{52}$$

where

$$\rho^2 = r^2 + a^2\cos^2\theta, \tag{53}$$

$$\Delta = r^2 - rR_S + a^2 + R_Q^2, \tag{54}$$

and

$$R_Q^2 = \frac{KGQ^2}{c^4}. \tag{55}$$

The term related to angular momentum is $a = J/Mc$. Three conservation constants of motions for a test particle of mass m and electric charge q can be obtained using Hamiltonian theory [65,66], which are

$$g_{\mu\nu}dx^\mu dx^\nu = -m^2c^2, \tag{56}$$

$$E = -\pi_t = -g_{tt}\dot{t} - g_{t\phi}\dot{\phi} + qA_t, \tag{57}$$

and

$$L = \pi_\phi = g_{\phi t}\dot{t} + g_{\phi\phi}\dot{\phi} - eA_\phi, \tag{58}$$

where the vector potential for electromagnetic fields is as follows [65–67,69]:

$$A = A_\mu dx^\mu = \frac{Qr}{\rho^2}\left(dt - a\sin^2\theta d\phi\right). \tag{59}$$

The equation of motion is

$$m\frac{Du^\mu}{D\tau} = eF^\mu_\nu u^\nu, \tag{60}$$

where $F^\mu_\nu = \partial_\nu A^\mu - \partial_\mu A^\nu$. Using the general form of the Hamilton–Jacobi equation, the following differential equations governing the motion of the charged test particle can be deduced [63–67,70]:

$$\rho^2\frac{dr}{d\lambda} = \pm P_R(r)^{1/2}, \tag{61}$$

$$\rho^2\frac{d\theta}{d\lambda} = \pm V^{1/2}, \tag{62}$$

$$\rho^2\frac{d\phi}{d\lambda} = -\frac{\left(aE\sin^2\theta - cL\right)}{\sin^2\theta} + \frac{a\left[E\left(r^2+a^2\right) - acL + KqQr\right]}{\Delta}, \tag{63}$$

and

$$\rho^2\frac{dt}{d\lambda} = \left(r^2+a^2\right)\left[E\left(r^2+a^2\right) - acL + KqQr\right] - \left(a^2E\sin^2\theta - acL\right), \tag{64}$$

where λ is the affine parameter related to the proper time τ of the particle divided by its mass m [63,67,70,71]; the Carter constant is zero here [63–65,70]:

$$P_R(r) = \left[E\left(r^2+a^2\right) - acL - KqQr\right]^2 - \Delta\left[m^2c^4r^2 + (cL - aE)^2\right], \tag{65}$$

and

$$V = \left[(cL - aE)^2 - m^2c^4a^2\sin^2\theta\right] - \left(\frac{aE\sin^2\theta - cL}{\sin\theta}\right)^2. \tag{66}$$

We consider the circular orbits in Figure 4, where the satisfied conditions are

$$P_R(r) = 0 \tag{67}$$

and

$$\frac{dP_R(r)}{dr} = 0. \tag{68}$$

Three orbital configurations have been discussed at $\theta = 0, \pi$, $\theta = \pi/2$, and $\theta = \pm\sqrt{\overline{K}/\overline{a}^2}$, where $\overline{K}$ and $\overline{a}$ are defined in [65]. Given the latitudinal equation of motion, it follows that the circular orbit passing through $\theta = 0$ and π only exists when $Q = 0$ [63,65]. Therefore, in our case of $Q \neq 0$, we simply consider the circular motion in the equatorial plane. In the case of particles with nonzero mass and a high specific charge, the above two

conditions for the circular orbitals give two good approximate solutions for E and L, which are shown below [63,65]:

$$E_{\pm} = \left(-\frac{KqQ}{r}\right)\frac{R_S r - 2a^2 - 2R_Q^2 \pm 2a\sqrt{r^2 - R_S r + a^2 + R_Q^2}}{2r^2 - 3R_S r + 4a^2 + 4R_Q^2 \pm 4a\sqrt{r^2 - R_S r + a^2 + R_Q^2}} \tag{69}$$

and

$$L_{\pm} = \left(-\frac{KqQ}{cr}\right)\frac{a\left(R_S r - 2a^2 - 2R_Q^2\right) \pm 2(r^2 - a^2)\sqrt{r^2 - R_S r + a^2 + R_Q^2}}{2r^2 - 3R_S r + 4a^2 + 4R_Q^2 \pm 4a\sqrt{r^2 - R_S r + a^2 + R_Q^2}}. \tag{70}$$

If the rotation of the charged test particle on the equatorial plane is counter-rotating, then the energy and angular momentum of the charged test particle are calculated with the sign "−" in the above two equations. Otherwise, the sign "+" is chosen if the charged test particle is corotating. In this metric, the frame-dragging effect is

$$\Omega = \frac{u^{\phi}}{u^t} = -\frac{g_{\phi t}}{g_{tt}}. \tag{71}$$

Although it exists in the Kerr–Newman source, the circular orbital can be corotating (prograde) and counter-rotating (retrograde) in the locally nonrotating frame [63,65,67,71]. Then, we can calculate the energy E and L by using the known a and R_Q. According to [55], the total charge $Q = 1.648824 \times 10^{20}$ C gives

$$R_Q = \sqrt{\frac{KGQ^2}{c^4}} = 0.4808\ R_S. \tag{72}$$

In our model, we consider electrons moving in circular orbitals on the equatorial plane, surrounding Region I at radius r between 0.9367 R_S and R_S. When Region I is static, the rotation term is a = 0, and the charged term is R_Q = 0.4808 R_S are used in the E and L calculations. The spacetime in Region I is described by the Kerr–Newman metric. Because the negative charges in Region II and Region III move ultra-relativistically surrounding Region I, the spacetime in and outside Region III is described by the Kerr–Newman metric. Therefore, the nonzero new rotation term a_{new} exists, which is produced by the surrounding negative charges. A simple choice of the negative charge in Region II and Region III is the electron, whose mass is very tiny and only 9.1×10^{-31} kg, so we consider electrons as the negative charges in Region II and Region III.

Next, we discuss how to construct a finite-size structure to satisfy the criterion of a Kerr–Newman black hole. The event horizons of the Kerr–Newman black hole, determined by $\Delta = 0$, are

$$r_{\pm} = \frac{R_S \pm \sqrt{R_S^2 - 4a_{new}^2 - 4R_{Q,new}^2}}{2}, \tag{73}$$

where r_- is the inner event horizon, and r_+ is the outer event horizon. If the Kerr–Newman black hole is expected, then it needs $r_+ \geq R_{\min} = 0.9367\ R_S$ at least. In order to reach this criterion, small and small a_{new} and $R_{Q,new}$ are better. Based on this, we use negative charges in Region II and Region III to balance the positive charges in Region I, so the term $R_{Q,new}$ can be reduced to zero. However, due to the surrounding electrons, the nonzero angular momentum of electrons gives rise to a nonzero a_{new}. For the purpose of decreasing the new rotation term a_{new}, both corotating and counter-rotating electrons are considered. The simple situation is that the corotating and counter-rotating electrons are equal, and their total charges are $Q_e = 1.648824 \times 10^{20}$ C. When the rotation term a of Region I and Region

II is zero, the angular momenta of the corotating and counter-rotating electrons are the same in magnitude, which are

$$L_{\pm}(a=0) = \pm\left(-\frac{KqQ}{cr}\right)\frac{2r^2\sqrt{r^2 - R_S r + R_Q^2}}{2r^2 - 3R_S r + 4R_Q^2}. \tag{74}$$

Therefore, if these two kinds of electrons are equal in number and move in opposite directions at very close orbitals, then the summation of their angular momenta is ~0. In the simple situation, we have $a_{new} \sim 0$ and $R_{Q,new} \sim 0$, so

$$r_+ = \frac{R_S + \sqrt{R_S^2 - 4a_{new}^2 - 4R_{Q,new}^2}}{2} \cong R_S > 0.9367R_S. \tag{75}$$

In this case, the event horizon is larger than the radius of Region III and includes Region I and Region II. The total number of electrons is $N = 1.029 \times 10^{39}$. As a result, a Kerr–Newman black hole with $a_{new} = 0$ and $R_{Q,new} = 0$, or a Schwarzschild black hole, is formed by using our model shown in Figure 4. In such a case, the radii of the counter-rotating and corotating electrons are denoted by r_1 and r_2, respectively. The radii satisfying $r_+ \geq \max(r_1, r_2)$ are drawn in Figure 5a, where the red points are the allowed radii for the whole structure, including Region I, Region II, and Region III, which can be black holes. More allowed radii are close to $R_{\min} = 0.9367\ R_S$, and the allowed radii decrease when they are close to R_S. On the other hand, the corresponding orbital energy and angular momentum for the counter-rotating (red) and corotating (green) electrons are plotted in Figure 5b,c, where the very small rotation term $a \leq 0.03\ R_S$ is considered with a constant $R_Q = 0.48\ R_S$, and the radii are between $0.938\ R_S$ and $1.007\ R_S$. Because the surrounding electrons are attracted by the positive charges, the orbital energy is negative, regardless of whether it is a counter-rotating or corotating electron. Both kinds of electrons have the same energy when $a = 0$. In Figure 5c, the angular momenta show that the counter-rotating electron has positive angular momentum, and the corotating electron has negative angular momentum by definition. When $a = 0$, both kinds of electrons have the same angular momentum in magnitude.

Not only the Schwarzschild black hole but also the Kerr–Newman black hole can be formed in our model. Next, we consider the occupation of the counter-rotating electrons is $\alpha_1 N$ and the occupation of the corotating electrons is $\alpha_2 N$, where $\alpha_1 \geq 0$ and $\alpha_2 \geq 0$, and $\alpha_1 + \alpha_2$ is not necessarily equal to one. If $\alpha_1 + \alpha_2 < 1$, the finite-size structure, including Region I, Region II, and Region III, is positively charged. Otherwise, if $\alpha_1 + \alpha_2 > 1$, the finite-size structure is negatively charged. Therefore, if $\alpha_1 + \alpha_2 \neq 1$, we have a nonzero total charge $Q_{new} = (1 - \alpha_1 - \alpha_2)Q$ and

$$R_{Q,new}^2 = \frac{KG(1-\alpha_1-\alpha_2)^2Q^2}{c^4} = (1-\alpha_1-\alpha_2)^2 R_Q^2. \tag{76}$$

If L_1 is the angular momentum of the counter-rotating electron and L_2 is the angular momentum of the corotating electron, then the total angular momenta are

$$L = \alpha_1 N L_1 + \alpha_2 N L_2, \tag{77}$$

and the new corresponding rotation term of the finite-size structure is

$$a_{new} = \frac{L}{[M + (\alpha_1 + \alpha_2)Nm_e]c} \cong \frac{L}{M_\odot c}. \tag{78}$$

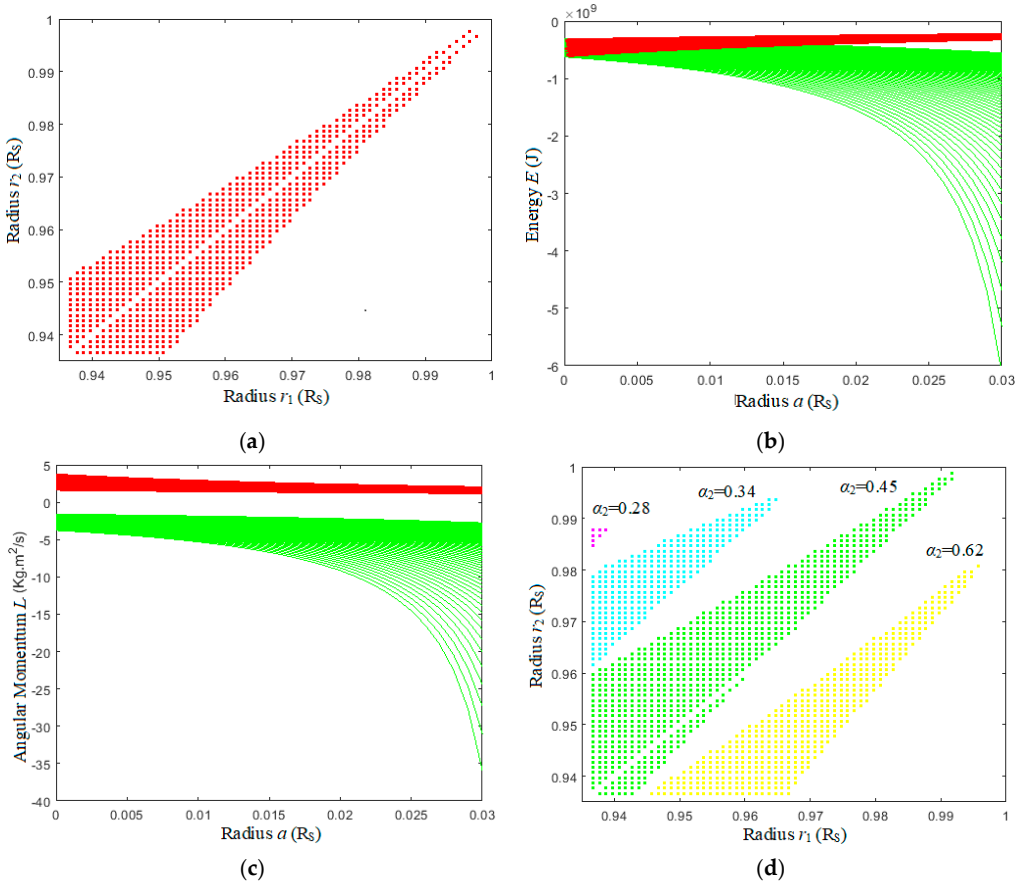

Figure 5. (**a**) When $\alpha_1 = \alpha_2 = 0.5$, the radii of the counter-rotating and corotating electrons, denoted by r_1 and r_2, respectively, satisfy $r_+ \geq \max(r_1, r_2)$ here. (**b**) The corresponding orbital energy for the counter-rotating (red) and corotating (green) electrons, where the very small rotation term $a \leq 0.03\ R_S$ is considered with a constant $R_Q = 0.48\ R_S$, and the radii are between $0.938\ R_S$ and $1.007\ R_S$, where both are plotted from up to down. (**c**) The corresponding angular momentum for the counter-rotating (red) and corotating (green) electrons are plotted in Figure 5b,c, where the very small rotation term $a \leq 0.03\ R_S$ is considered with a constant $R_Q = 0.48\ R_S$, and the radii are between $0.938\ R_S$ and $1.007\ R_S$, where the red parts are plotted from down to up, and the green parts are plotted from up to down. (**d**) When $\alpha_1 = 0.5$ and four α_2 values, 0.28 (purple), 0.34 (cyan), 0.45 (green), and 0.62 (yellow), are chosen, the allowed radii r_1 and r_2 satisfying $r_+ \geq \max(r_1, r_2)$ are plotted. As α_2 increases, the trend of the allowed r_2 decreases at the same r_1.

In order to have a small a_{new}, the values of α_1 and α_2 are expected to be close to each other. Some allowed radii of the counter-rotating and corotating electrons are plotted in Figure 5d, where α_1 is fixed at 0.50, and four different α_2 values, 0.28 (purple), 0.34 (cyan), 0.45 (green), and 0.62 (yellow), are chosen. As α_2 increases, the trend of the allowed r_2 decreases at the same r_1. In this case, of $\alpha_1 = 0.50$, the minimum α_2 is 0.277 by our calculations. In conclusion, our model can construct a black hole, and the property of the black hole is dominated by the corotating and counter-rotating electrons, which makes the black hole charged or uncharged and rotating or non-rotating.

Furthermore, the Schwarzschild radius is linearly proportional to $m(R_S) = M$, so the average density of a black hole is

$$\bar{\rho} = \frac{3c^6}{32\pi G^3 M^2}. \tag{79}$$

This shows that the average density is inversely proportional to the total mass square. Therefore, the higher the average density is, the lower the total mass and radius.

2.6. Energy Conservation Between Different Energy Transformations

In the following section, we consider the possible size of a neutron star. Due to the supernova producing ultra-high pressure, $2N$ neutrons are supposed to be produced. Because of the supernova, in fact, αN neutrons transfer to the radiation energy and work to compress the materials, and $(2-\alpha)N$ neutrons are left there. The volume is changed from V_0 to V, and the radius from R to $R^{'}$. Then, the total kinetic energy of the rest $(2-\alpha)N$ neutrons within the volume V in the ultra-relativistic condition is as follows [46]:

$$U_N \approx \frac{2\pi V m_n^4 c^5}{h^3}\left(\frac{p_f}{m_n c}\right)^4 = \frac{2\pi V c p_f^4}{h^3} = \frac{3(2-\alpha)Nhc}{4}\left[\frac{3(2-\alpha)N}{8\pi V}\right]^{1/3}, \tag{80}$$

where the momentum of the Fermi energy for the neutron gas is

$$p_f = h\left[\frac{3(2-\alpha)N}{8\pi V}\right]^{1/3}. \tag{81}$$

Finally, the total energy of these $(1-\alpha)N$ and $(2-\alpha)N$ neutrons approximates to

$$\begin{aligned} U_{total}^{rest} &\approx U_N + (1-\alpha)Nm_e c^2 + (2-\alpha)Nm_n c^2 + U_g^{rest} \\ &\approx \tfrac{3(2-\alpha)Nhc}{4}\left[\tfrac{3(2-\alpha)N}{8\pi V}\right]^{1/3} + (1-\alpha)Nm_e c^2 + (2-\alpha)Nm_n c^2 + U_g^{rest}, \end{aligned} \tag{82}$$

where the self-energy of gravity forming those $(2-\alpha)N$ neutrons in the homogeneous density distribution is

$$U_g^{rest} = \frac{3G(2-\alpha)^2 m_n^2 N^2}{5}\left(\frac{4\pi}{3V}\right)^{1/3}. \tag{83}$$

Similarly, when we consider the inhomogeneous case, then the gravitational self-energy of the star with a radius of $R^{'}$ is

$$U_g^{rest} = \int_0^{R'} 4\pi c^2 \rho(r)\frac{\left[1-e^{-\lambda(r)}\right]}{2}dr = \int_0^{R'} \frac{G4\pi r^2\rho(r)dr}{r}\int_0^r 4\pi r'^2\rho(r')dr', \tag{84}$$

where $R' < R$, and $e^{-\lambda(r)}$ is the metric potential in Equation (1). Considering energy conservation, it yields

$$U_{total}^{rest} < \frac{3(2N)hc}{4}\left[\frac{3(2N)}{8\pi V_0}\right]^{1/3} + Nm_e c^2 + 2Nm_n c^2 + U_g < \infty. \tag{85}$$

Equation (85) clearly shows that $V > 0$ and $V < V_0$, so the $(2-\alpha)N$ neutrons form a finite-size volume, and they cannot shrink to a point.

2.7. The Upper Limit of the Core Size in the Black Hole

In fact, it has been revealed that the upper-mass limit of the white dwarf star, calculated using the homogeneous density model, is close to the inhomogeneous density model by considering $\mathrm{d}p/\mathrm{d}r$ and $\mathrm{d}m/\mathrm{d}r$ [45,46]. The correction involves multiplying the self-energy in the homogeneous density model by a constant of 1.124 [45,46]. In such a compact star, the homogeneous density model is a good approximation. Therefore, we can adopt the homogeneous density in both Equations (14) and (84) for the compact star. Furthermore, by ignoring the total energy of the remaining electrons, Equation (85) yields

$$\begin{aligned} \alpha N m_n c^2 + &\left[2(2)^{1/3} - (2-\alpha)(2-\alpha)^{1/3}\left(\tfrac{1}{\beta}\right)^{1/3}\right]\tfrac{3Nhc}{4}\left(\tfrac{3N}{8\pi V_0}\right)^{1/3} \\ &+ \tfrac{3Gm_n^2N^2}{5}\left[4-(2-\alpha)^2\left(\tfrac{1}{\beta}\right)^{1/3}\right]\left(\tfrac{4\pi}{3V_0}\right)^{1/3} > 0, \end{aligned} \tag{86}$$

where $V = \beta V_0$ with $0 < \beta < 1$. When α is small, and considering the Taylor expansion to the linear term for $(2-\alpha)^{1/3}$, Equation (86) becomes

$$\begin{aligned}\alpha N m_n c^2 + 2(2)^{1/3}\left[1-\left(1-\tfrac{\alpha}{2}\right)\left(1-\tfrac{\alpha}{6}\right)\left(\tfrac{1}{\beta}\right)^{1/3}\right]\tfrac{3Nhc}{4}\left(\tfrac{3N}{8\pi V_0}\right)^{1/3} \\ + \tfrac{3Gm_n^2N^2}{5}\left[4-\left(4-4\alpha+\alpha^2\right)\left(\tfrac{1}{\beta}\right)^{1/3}\right]\left(\tfrac{4\pi}{3V_0}\right)^{1/3} > 0.\end{aligned} \tag{87}$$

After arranging the above equation, it yields

$$\begin{aligned}\alpha m_n c^2(\beta)^{1/3} + 2\left[(\beta)^{1/3} - 1 + \tfrac{2}{3}\alpha - \tfrac{1}{12}\alpha^2\right]\tfrac{3hc}{4}\left(\tfrac{3N}{4\pi V_0}\right)^{1/3} \\ + \tfrac{3}{5}Gm_n^2N\left[4(\beta)^{1/3} - \left(4-4\alpha+\alpha^2\right)\right]\left(\tfrac{4\pi}{3V_0}\right)^{1/3} > 0.\end{aligned} \tag{88}$$

Then, solving α, the range is

$$\begin{aligned}\max\left\{0, \frac{\left\{-(\textit{square root term})+\left[m_nc^2(\beta V_0)^{1/3}+hc\left(\frac{3N}{4\pi}\right)^{1/3}+\frac{12}{5}Gm_n^2N\left(\frac{4\pi}{3}\right)^{1/3}\right]\right\}}{\left[\frac{hc}{4}\left(\frac{3N}{4\pi}\right)^{1/3}+\frac{6}{5}Gm_n^2N\left(\frac{4\pi}{3}\right)^{1/3}\right]}\right\} < \alpha \\ < \min\left\{2, \frac{\left\{(\textit{square root term})+\left[m_nc^2(\beta V_0)^{1/3}+hc\left(\frac{3N}{4\pi}\right)^{1/3}+\frac{12}{5}Gm_n^2N\left(\frac{4\pi}{3}\right)^{1/3}\right]\right\}}{\left[\frac{hc}{4}\left(\frac{3N}{4\pi}\right)^{1/3}+\frac{6}{5}Gm_n^2N\left(\frac{4\pi}{3}\right)^{1/3}\right]}\right\},\end{aligned} \tag{89}$$

where the square root term is

$$\begin{aligned}&\textit{square root term} \\ &= \left\{\left[m_nc^2(\beta V_0)^{1/3} + hc\left(\tfrac{3N}{4\pi}\right)^{1/3} + \tfrac{12}{5}Gm_n^2N\left(\tfrac{4\pi}{3}\right)^{1/3}\right]^2\right. \\ &- 4\left[\tfrac{hc}{8}\left(\tfrac{3N}{4\pi}\right)^{1/3} + \tfrac{3}{5}Gm_n^2N\left(\tfrac{4\pi}{3}\right)^{1/3}\right]\left[\tfrac{3hc}{2}\left(\tfrac{3N}{4\pi}\right)^{1/3}\right. \\ &\left.\left.+ \tfrac{12}{5}Gm_n^2N\left(\tfrac{4\pi}{3}\right)^{2/3}\right]\left[1-(\beta)^{1/3}\right]\right\}^{1/2}.\end{aligned} \tag{90}$$

This square root term depends on N, β, and V_0. All other parameters are well-known constants. This α range approximately gives the exhaust of neutron particles in the event of a supernova. Equation (89) can estimate the mass of a black hole and its core volume by considering the number of neutrons in the original star.

Then, according to Equation (90), we demonstrate two situations and theoretically study the trend between the low limit α and β, as shown in Figure 6. The first situation is the star radius r equal to $R_\odot$, in which three cases of $2M_\odot$, $3M_\odot$, and $4M_\odot$ are considered in this situation. In our calculations, three curves for the three cases of the first situation are plotted in Figure 6—indigo ($2M_\odot$), green ($3M_\odot$), and red ($4M_\odot$) curves from left to right. These three cases are also circled and denoted by $r = R_\odot$. The other three cases for the second situation, circled and denoted by $r = 0.1\ R_\odot$ in Figure 6, are the indigo, green, and red curves corresponding to $2M_\odot$, $3M_\odot$, and $4M_\odot$ from left to right. The radius of each star in the first situation is 10 times larger than that of each star in the second situation. Therefore, in the second situation, the density of the star is 1000 times larger than that of the star with the same mass in the first situation. In both situations, the curves of the lightest star ($2M_\odot$) are leftmost, and the curves of the heaviest star ($4M_\odot$) are rightmost. In these curves, the low limit α means the minimum exhausting energy, and β represents the ratio of the final volume to the initial volume for each star experiencing a supernova. If a smaller final volume is expected after a supernova, the exhausting energy has to be greater than that of the larger final volume because a lot of exhausting energy is used to compress the initial volume to a smaller final one. In Figure 6, the low-limit α increases from 10% to 90% when β decreases from about 10^{-13} to 10^{-19} for the 4-$M_\odot$ case of the first situation, and

from about 10^{-10} to 10^{-16} for the same case of the second situation. Theoretically speaking, the denser star needs more energy to compress itself to a smaller volume than a less dense star. For example, exhausting 10% mass or considering the low limit α= 0.2 can reach a much smaller β of about 10^{-13} in the first situation than in the second situation, where β is about 10^{-10}, a much higher value. All these results are obtained by considering energy conservation.

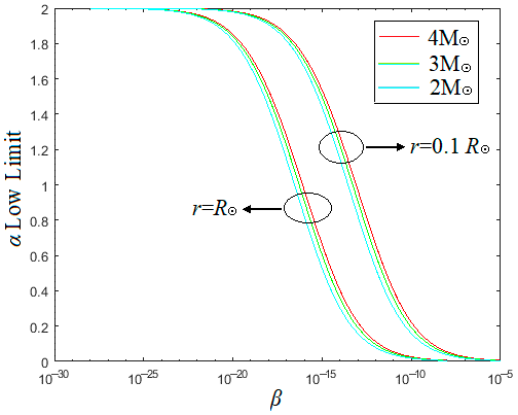

Figure 6. A comparison between α and β according to Equation (90). There are two groups plotted, and the right group is 1000 times denser than the left group. Each group includes three cases where the mass of the star is $2M_\odot$, $3M_\odot$, and $4M_\odot$ from left to right, and the radius of the star is the same in each case. The results show that the denser star wastes more energy to reduce its size at the same final volume.

Recently, the similarity between the neutron star and the black hole has been discussed [47]. The compression of neutrons and helium atoms under extreme pressure has been studied [72,73]. Neutrons and protons are both baryons composed of quarks and gluons. They have much ability to change their sizes, and the force inside them is a strong interaction that is 10^{39} times larger than gravity. The experiment on the distribution of pressure inside the proton also showed an average peak pressure of about 10^{35} Pascals near the center of a proton [34]. This pressure greatly exceeds the pressure estimated by most neutron stars. When we compress the remaining $(2-\alpha)N$ neutrons, they become much smaller, as shown in the quark-matter phase diagrams [74,75], and all the volume V is within the event horizon of a black hole. In our discussions, we want to reveal the truth that the so-called curvature singularity inside the black hole, such as $r = 0$ in the Schwarzschild black hole, is a mathematical concept in the Schwarzschild metric that is not rooted in a physical foundation. In traditional black hole theory, everything inside the black hole inevitably reaches $r = 0$ due to strong gravity, without considering any physical reality, and energy input and output. The evolution from a star to a black hole should follow energy conservation, and the black hole reasonably has a finite-size nucleus in it, not a singularity.

3. Conclusions

In summary, the reasonableness of the singularity of the black hole is studied in this paper. When we consider that everything in the black hole collects at a singularity, the infinite density of mass, charge, gravitational energy, and electric energy is very nonphysical. This gives rise to a question about why all masses, as well as all charges, gather at a point. However, a black hole can evolve from a star with finite energy. Such a structure does not obey energy conservation laws. If we believe in the singularity in the black hole, we believe in the knowledge of the 1920s or 1930s, 100 years ago. At that time, people still did not have deep ideas about neutrons, and they did not even know what a strong interaction and quarks were. They just treated a mathematical solution as a real physical object without

any believable proof of its physical truth. When we put the black hole and the Big Bang together, we see very clearly that the singularity is a contradictory concept. The ultra-super strong gravity of the singularity before the Big Bang affects the explosion and stops the expansion of the universe.

Regarding singularity, an example of charged electrons is used to check whether the singularity exists or not. The result clearly shows that regardless of how large the energy of the charged electrons is, those electrons are very hard to shrink to a point, physically speaking. They always have finite volumes discussed in statistical mechanics. The singularity also tells us that gravitational energy and Coulomb's energy are infinite there. Since many black holes evolve from stars with finite energy, it is unreasonable to have infinite energy for black holes. We also use a case of 1.4×10^{31} Coulomb electrons at infinity to demonstrate that to collect those electrons in a sphere with a radius of 50 m requires 2.114×10^{70} Joules, which is more than the energy in the observable universe. In such a case, the distance between two electrons is larger than 10^{-15} m, whereas classical electrodynamics is still useful. This case tells us that the traditional concept of gravitational collapse cannot shrink those electrons to a singularity, and the process of the collection is physical. We have to put in a lot of energy to gather those electrons in a small space. Hence, the charged sources described by Kerr or Kerr–Newman metrics are not small in terms of space because Coulomb's force acts against the shrinking process. Thus, we use neutron gases as the most likely constituents after a supernova to discuss their volume based on energy conservation. The result is similar to what we already know about Fermi electron gas. So, theoretically speaking, a black hole has a finite-size nucleus inside it, not a singularity.

One important note for this paper is that a complex structure of a double-characteristic black hole is proposed, where the total charge can be zero or nonzero. This kind of black hole has a positively charged Region I, possibly consisting of neutrons with a few Fe nuclei, which is surrounded by negative charges moving corotating or counter-rotating, denoted by Region II and Region III. We follow the report with the finding that a charged and non-rotating compact star with a mass of a solar mass and a radius of 0.9367 *Rs* can have a charge as high as 1.648824×10^{20} Coulombs. Adopting these quantities in our model, the spacetime in Region I is described by the Kerr–Newman metric. Within the outermost layer, the spacetime is described by the Kerr–Newman metric, and the place outside the outermost layer is also described by the Kerr–Newman metric. The counter-rotating and corotating electrons in Region II and Region III can make the whole structure charged or uncharged and rotating or non-rotating. Some allowed radii of the counter-rotating and corotating electrons are given to reach the whole structure within the outer event horizon of the Kerr–Newman black hole. Due to this structure, it reaches $r_+ \geq \max(r_1, r_2)$, so the black hole is formed by our model. A simple case yields a Schwarzschild black hole when both the counter-rotating and corotating electrons are equal, move on very close orbitals, and the total charge of the whole structure is zero. In such a case, a finite-size structure in the Kerr–Newman metric transforms into a Schwarzschild black hole. To sum up, our model can construct black holes, and the properties of the black holes are dominated by corotating and counter-rotating electrons, which make the black holes charged or uncharged and rotating or non-rotating.

Funding: This research received no external funding before publication.

Data Availability Statement: All data that support the findings of this study are included within the article.

Acknowledgments: The author thanks the reviewers for their helpful comments.

Conflicts of Interest: The author declares no conflicts of interests.

References

1. Miyoshi, M.; Moran, J.; Herrnstein, J.; Greenhill, L.; Nakai, N.; Diamond, P.; Inoue, M. Evidence for a black hole from high rotation velocities in a sub-parsec region of NGC4258. *Nature* **1995**, *373*, 127–129. [CrossRef]
2. Miller, J.M.; Raymond, J.; Reynolds, C.S.; Fabian, A.C.; Kallman, T.R.; Homan, J. The Accretion Disk Wind in the Black Hole GRO J1655−40. *Astrophys. J.* **2008**, *680*, 1359–1377. [CrossRef]
3. McHardy, I.M.; Gunn, K.F.; Uttley, P.; Goad, M.R. MCG-6-30-15: Long time-scale X-ray variability, black hole mass and active galactic nuclei high states. *Mon. Not. R. Astron. Soc.* **2005**, *359*, 1469–1480. [CrossRef]
4. van Dokkum, P.; Pasha, I.; Buzzo, M.L.; LaMassa, S.; Shen, Z.; Keim, M.A.; Abraham, R.; Conroy, C.; Danieli, S.; Mitra, K.; et al. A Candidate Runaway Supermassive Black Hole Identified by Shocks and Star Formation in its Wake. *Astrophys. J.* **2023**, *946*, L50. [CrossRef]
5. Abbott, B.P.; Abbott, R.; Abbott, T.D.; Abernathy, M.R.; Acernese, F.; Ackley, K.; Adams, C.; Adams, T.; Addesso, P.; Adhikari, R.X.; et al. Observation of Gravitational Waves from a Binary Black Hole Merger. *Phys. Rev. Lett.* **2016**, *116*, 061102. [CrossRef]
6. Abbott, B.P.; Abbott, R.; Abbott, T.D.; Abernathy, M.R.; Acernese, F.; Ackley, K.; Adams, C.; Adams, T.; Addesso, P.; Adhikari, R.X.; et al. GW151226: Observation of Gravitational Waves from a 22-Solar-Mass Binary Black Hole Coalescence. *Phys. Rev. Lett.* **2016**, *116*, 241103. [CrossRef]
7. Abbott, B.P.; Abbott, R.; Abbott, T.D.; Acernese, F.; Ackley, K.; Adams, C.; Adams, T.; Addesso, P.; Adhikari, R.X.; Adya, V.B.; et al. GW170104: Observation of A 50 Solar-Mass Binary Black Hole Coalescence at Redshift 0.2. *Phys. Rev. Lett.* **2017**, *118*, 221101. [CrossRef]
8. Abbott, B.P.; Abbott, R.; Abbott, T.D.; Acernese, F.; Ackley, K.; Adams, C.; Adams, T.; Addesso, P.; Adhikari, R.X.; Adya, V.B.; et al. GW170814: A Three-Detector Observation of Gravitational Waves from A Binary Black Hole Coalescence. *Phys. Rev. Lett.* **2017**, *119*, 141101. [CrossRef] [PubMed]
9. Abbott, B.P.; Abbott, R.; Abbott, T.D.; Acernese, F.; Ackley, K.; Adams, C.; Adams, T.; Addesso, P.; Adhikari, R.X.; Adya, V.B.; et al. GW170817: Observation of Gravitational Waves from A Binary Neutron Star Inspiral. *Phys. Rev. Lett.* **2017**, *119*, 161101. [CrossRef]
10. Pei, T.-H. The Black Hole with A Finite Size Based on Energy Conservation, Coulomb's Force, and Strong Interaction. *Int. J. Sci. Eng. Res.* **2019**, *10*, 661–669.
11. Schutz, B.F. *A First Course in General Relativity*; Cambridge University Press: Cambridge, UK, 1985; p. 291.
12. Ohanian, H.C.; Ruffini, R. *Gravitation and Spacetime*, 2nd ed.; W. W. Norton & Company: New York, NY, USA, 1994; pp. 445–449.
13. De Felice, F.; Clarke, C.J.S. *Relativity on Curved Manifolds*; Cambridge University Press: Cambridge, UK, 1990; pp. 355–362.
14. Stephani, H. *Relativity-An Introduction to Special and General Relativity*, 3rd ed.; Cambridge University Press: Cambridge, UK, 2004; p. 303.
15. Mould, R.A. *Basic Relativity*; Springer: New York, NY, USA, 2002; p. 324.
16. Misner, C.W.; Thorne, K.S.; Wheeler, J.A. *Gravitation*; W. H. Freeman and Company: New York, NY, USA, 1970; p. 880.
17. The Event Horizon Telescope Collaboration; Akiyama, K.; Alberdi, A.; Alef, W.; Asada, K.; Azulay, R.; Baczko, A.-K.; Ball, D.; Baloković, M.; Barrett, J.; et al. First M87 Even Horizon Telescope Results. I. The Shadow of the Supermassive Black Hole. *Astrophys. J. Lett.* **2019**, *875*, L1.
18. Alexander, T.; Natarajan, P. Rapid growth of seed black holes in the early universe by supra-exponential accretion. *Science* **2014**, *345*, 1330–1333. [CrossRef]
19. Latif, M.A.; Ferrara, A. Formation of Supermassive Black Hole Seeds. *Publ. Astron. Soc. Aust.* **2016**, *33*, e051. [CrossRef]
20. Ricarte, A.; Natarajan, P. The Observable Signatures of Massive Black Hole Seeds. *Mon. Not. Roy. Astro. Soc.* **2018**, *481*, 3278–3292. [CrossRef]
21. Nicolini, P. A model of radiating black hole in noncommutative geometry. *J. Phys. A Math. Gen.* **2005**, *38*, L631–L638. [CrossRef]
22. Nicolini, P.; Smailagic, A.; Spallucci, E. Noncommutative geometry inspired Schwarzschild black hole. *Phys. Lett. B* **2006**, *632*, 547–551. [CrossRef]
23. Ansoldi, S.; Nicolini, P.; Smailagic, A.; Spallucci, E. Non-commutative geometry inspired charged black holes. *Phys. Lett. B* **2007**, *645*, 261–266. [CrossRef]
24. Smailagic, A.; Spallucci, E. "Kerrr" black hole: The lord of the string. *Phys. Lett. B* **2010**, *688*, 82–87. [CrossRef]
25. Modesto, L.; Nicolini, P. Charged rotating noncommutative black holes. *Phys. Rev. D* **2010**, *82*, 104035. [CrossRef]
26. Spallucci, E.; Smailagic, A.; Nicolini, P. Non-commutative geometry inspired higher-dimensional charged black holes. *Phys. Lett. B* **2009**, *670*, 449–454. [CrossRef]
27. Nicolini, P.; Spallucci, E. Non-Commutative Geometry Inspired Dirty Black Holes. *Class. Quantum Gravity* **2009**, *27*, 015010. [CrossRef]

28. Nicolini, P. Noncommutative black holes, the final appeal to quantum gravity: A review. *Int. J. Mod. Phys. A* **2009**, *24*, 1229–1308. [CrossRef]
29. Visser, M. The Kerr Spacetime: A Brief Introduction. Available online: https://arxiv.org/pdf/0706.0622.pdf (accessed on 15 June 2008).
30. Venkataraman, G. *Chandrasekhar and His Limit*; Universities Press: Hyderabad, India, 1992; p. 89.
31. Pei, T.-H. The Highly Accurate Relation Between the Radius and Mass of the White Dwarf Star From Zero to Finite Temperature. *Front. Astron. Space Sci.* **2022**, *8*, 799210. [CrossRef]
32. Oppenheimer, J.R.; Vokff, G.M. On Massive Neutron Core. *Phys. Rev.* **1939**, *55*, 374. [CrossRef]
33. Heiselberg, H.; Pandharipande, V. Recent Progress in Neutron Star Theory. *Annu. Rev. Nucl. Part. Sci.* **2000**, *50*, 481–524. [CrossRef]
34. Kalogera, V.; Baym, G. The Maximum Mass of a Neutron Star. *Astrophys. J.* **1996**, *470*, L61–L64. [CrossRef]
35. Burkert, V.D.; Elouadrhiri, L.; Girod, F.X. The pressure distribution inside the proton. *Nature* **2018**, *557*, 396–399. [CrossRef] [PubMed]
36. Fukugita, M.; Peebles, P.J.E. The Cosmic Energy Inventory. *Astrophys. J.* **2004**, *616*, 643–668. [CrossRef]
37. Feynman, R.P.; Leighton, R.B.; Sands, M. *The Feynman Lectures on Physics–The New Millennium Edition-Volume II: Mainly Electromagnetism and Matter*; Basic Books: New York, NY, USA, 1964; pp. 5–7.
38. Arbañil, J.D.V.; Lemos, J.P.S.; Zanchin, V.T. Incompressible relativistic spheres: Electrically charged stars, compactness bounds, and quasiblack hole configurations. *Phys. Rev. D* **2014**, *89*, 104054. [CrossRef]
39. Lemos, J.P.S.; Lopes, F.J.; Quinta, G.; Zanchin, V.T. Compact stars with a small electric charge: The limiting radius to mass relation and the maximum mass for incompressible matter. *Eur. Phys. J. C* **2015**, *75*, 76. [CrossRef]
40. Sharif, M.; Butt, I.I. Complexity factor for charged spherical system. *Eur. Phys. J. C* **2018**, *78*, 688. [CrossRef]
41. Jasim, M.; Maurya, S.; Ray, S.; Shee, D.; Deb, D.; Rahaman, F. Charged strange stellar model describing by Tolman V metric. *Results Phys.* **2021**, *20*, 103648. [CrossRef]
42. Ray, S.; Espindola, A.L.; Malheiro, M.; Lemos, J.P.; Zanchin, V.T. Electrically Charged Compact Stars and Formation of Charged Black Holes. *Phys. Rev. D* **2003**, *68*, 084004. [CrossRef]
43. Maurya, S.K.; Banerjee, A.; Channuie, P. Relativistic compact stars with charged anisotropic matter. *Chin. Phys. C* **2018**, *42*, 055101. [CrossRef]
44. Pei, T.-H. The Superluminal Phenomenon of Light Near the Kerr-Newman Black Hole or Super-Gravitational Source. *Front. Phys.* **2021**, *9*, 701619. [CrossRef]
45. Huang, K. *Statistical Mechanics*, 2nd ed.; John Weily & Sons, Inc.: Hoboken, NJ, USA, 1987; p. 247.
46. Greiner, W.; Neise, L.; Stöcker, H. *Thermodynamics and Statistical Mechanics*; Springer: New York, NY, USA, 1995; p. 355.
47. Sher, A. Is A Black Hole A Neutron Star? Available online: http://vixra.org/abs/1806.0329 (accessed on 12 September 2024).
48. de Carvalho, S.M.; Rotondo, M.; Rueda, J.A.; Ruffini, R. Relativistic Feynman-Metropolis-Teller treatment at finite temperatures. *Phys. Rev. C* **2014**, *89*, 015801. [CrossRef]
49. Boshkayev, K.A.; Rueda, J.A.; Zhami, B.; Kazymova, Z.A.; Balgymbekov, G.S. Equilibrium Structure of White Dwarfs at Finite Temperatures. *Int. J. Mod. Phys. Conf. Ser.* **2015**, *41*, 1660129. [CrossRef]
50. Lobato, R.V.; Carvalho, G.A.; Kelkar, N.G.; Nowakowski, M. Mssive White Dwarfs in f(R,Lm) gravity. *Eur. Phys. J. C* **2022**, *82*, b540. [CrossRef]
51. Lattimer, J.M. The Nuclear Equation of State and Neutron Star Masses. *Annu. Rev. Nucl. Part. Sci.* **2012**, *62*, 485–515. [CrossRef]
52. Steiner, A.W.; Lattimer, J.M.; Brown, E.F. Neutron Star Radii, Universal Relation, and the Role of Prior Distributions. *Eur. Phys. J. A* **2016**, *52*, 18. [CrossRef]
53. Özel, F.; Psaltis, D. Reconstructing the neutron-star equation of state from astrophysical measurements. *Phys. Rev. D* **2009**, *80*, 103003. [CrossRef]
54. Read, J.S.; Lackey, B.D.; Owen, B.J.; Friedman, J.L. Constraints on A Phenomenologically Parametrized Neutron-Star Equation of State. *Phys. Rev. D* **2009**, *79*, 124032. [CrossRef]
55. Estevez-Delgado, G.; Estevez-Delgado, J.; Pineda Duran, M.; Montelongo García, N.; Paulin-Fuentes, J.M. A charged perfect fluid model with high compactness. *Rev. Mex. F ´ısica* **2019**, *65*, 382–391. [CrossRef]
56. Negreiros, R.P.; Weber, F.; Malheiro, M.; Usov, V. Electrically Charged Strange Quark Stars. *Phys. Rev. D* **2009**, *80*, 083006. [CrossRef]
57. Dayanandan, B.; Maurya, S.K. Modelling of Charged Anisotropic Compact Stars in General Relativity. *Eur. Phys. J. A* **2017**, *53*, 141. [CrossRef]
58. Gedela, S.; Pant, N.; Upreti, J.; Pant, R.P. A New Parametric Class of Solutions of A Charged Anisotropic Compact Star via Bardeen Exterior Geometry. *Mod. Phys. Lett. A* **2021**, *36*, 2150055. [CrossRef]
59. Pretel, J.M.; Banerjee, A.; Pradhan, A. Electrically Charged Quark Stars in 4D Einstein-Gauss-Bonett Gravity. *Eur. Phys. J. C* **2022**, *82*, 180. [CrossRef]

60. Pei, T.-H. The Additional Pressure of White Dwarf Stars Generated by Net Charges. *Publ. Astron. Soc. Jpn.* **2023**, *75*, 893–906. [CrossRef]
61. Andréasson, H. Sharp bounds on the critical stability radius for relativistic charged spheres. *Commun. Math. Phys.* **2008**, *288*, 715–730. [CrossRef]
62. Adamo, T.; Newman, E.T. The Kerr-Newman Metric: A Review. *arXiv* **2014**, arXiv:1410.6626.
63. Balek, V.; Bicak, J.; Stuchlik, Z. The motion of the charged particles in the field of rotating charged black holes and naked singularities. II-The motion in the equatorial plane. *Astron. Inst. Czechoslov. Bull.* **1989**, *40*, 133–165.
64. Bicak, J.; Stuchlik, Z.; Balek, V. The motion of charged particles in the field of rotating charged black holes and naked singularities. *Astron. Inst. Czechoslov. Bull.* **1989**, *40*, 65–92.
65. Hackmann, E.; Xu, H. Charged particle motion in Kerr-Newmann space-times. *Phys. Rev. D* **2013**, *87*, 124030. [CrossRef]
66. Heisnam, S.; Meitei, I.A.; Singh, K.Y. Motion of a Test Particle in the Kerr-Newman De/Anti De Sitter Space-Time. *Int. J. Astron. Astrophys.* **2014**, *4*, 365–373. [CrossRef]
67. Cebeci, H.; Özdemir, N.; Şentorun, S. The Equatorial Motion of Charged Test Particles in Kerr-Newman-Taub-NUT Spacetime. *Gen. Relativ. Gravit.* **2019**, *51*, 84. [CrossRef]
68. Pei, T.-H. The Average Radial Speed of Light From Near to Far Space Surrounding the Kerr–Newman Super-Gravitational Source. *Front. Astron. Space Sci.* **2022**, *9*, 878156. [CrossRef]
69. Pugliese, D.; Quevedo, H.; Ruffini, R. Equatorial circular orbits of neutral test particles in the Kerr-Newman spacetime. *Phys. Rev. D* **2013**, *88*, 024042. [CrossRef]
70. Liu, C.-Y.; Lee, D.-S.; Lin, C.-Y. Geodesic motion of neutral particles around a Kerr–Newman black hole. *Class. Quantum Gravity* **2017**, *34*, 235008. [CrossRef]
71. Pradhan, P. Circular geodesics in the Kerr–Newman–Taub–NUT spacetime. *Class. Quantum Gravity* **2015**, *32*, 165001. [CrossRef]
72. Llanes-Estrada, F.J.; Navarro, G.M. Cubic Neutrons. *Mod. Phys. Lett. A* **2012**, *27*, 1250033. [CrossRef]
73. Portela, P.C.; Llanes-Estrada, F.J. Cubic Wavefunction Deformation of Compressed Atoms. *Few-Body Syst.* **2015**, *56*, 231–240. [CrossRef]
74. Alford, M.G.; Schmitt, A.; Rajagopal, K.; Schäfer, T. Color superconductivity in dense quark matter. *Rev. Mod. Phys.* **2008**, *80*, 1455–1515. [CrossRef]
75. Fukushima, K.; Hatsuda, T. The Phase Diagram of Dense QCD. *Rep. Prog. Phys.* **2011**, *74*, 014001. [CrossRef]